

# Optimal Control of the Strong-Field Ionization of Silver Clusters in Helium Droplets

N. X. Truong<sup>1</sup>, P. Hilse<sup>2</sup>, S. Göde<sup>1</sup>, A. Przystawik<sup>1</sup>, T. Döppner<sup>1</sup>, Th. Fennel<sup>1</sup>,  
Th. Bornath<sup>1</sup>, J. Tiggesbäumker<sup>1</sup>, M. Schlanges<sup>2</sup>, G. Gerber<sup>3</sup>, and K. H. Meiwes-Broer<sup>1</sup>

<sup>1</sup> *Institut für Physik, Universität Rostock, 18051 Rostock, Germany*

<sup>2</sup> *Institut für Physik, Ernst-Moritz-Arndt-Universität Greifswald, 17489 Greifswald, Germany and*

<sup>3</sup> *Physikalisches Institut, Universität Würzburg, 97074 Würzburg, Germany \**

(Dated: August 6, 2018)

Optimal control techniques combined with femtosecond laser pulse shaping are applied to steer and enhance the strong-field induced emission of highly charged atomic ions from silver clusters embedded in helium nanodroplets. With light fields shaped in amplitude and phase we observe a substantial increase of the  $\text{Ag}^{q+}$  yield for  $q > 10$  when compared to bandwidth-limited and optimally stretched pulses. A remarkably simple double-pulse structure, containing a low-intensity prepulse and a stronger main pulse, turns out to produce the highest atomic charge states up to  $\text{Ag}^{20+}$ . A negative chirp during the main pulse hints at dynamic frequency locking to the cluster plasmon. A numerical optimal control study on pure silver clusters with a nanoplasma model converges to a similar pulse structure and corroborates, that the optimal light field adapts to the resonant excitation of cluster surface plasmons for efficient ionization.

PACS numbers: 36.40.Gk, 52.50.Jm

## I. INTRODUCTION

Atomic clusters in intense laser pulses have received considerable attention since the mid-90's because of the potential for several promising applications, such as the controlled generation of highly charged atomic ions [1], energetic electrons [2], x-rays [3], or even nuclear particles [4]. Besides technological interest, the absence of hidden dissipation channels makes clusters to a valuable testing ground for exploring many-particle effects in strong-field laser-matter interactions [5].

A remarkable feature of clusters exposed to intense near-infrared (NIR) femtosecond laser pulses is the extremely efficient absorption of radiation energy due to the coupling of the light field to a dense transient nanoplasma [6]. The resulting highly nonlinear cluster response has been studied theoretically by several groups and it is widely accepted that resonant collective electron heating by excitation of Mie surface plasmons is a key mechanism for high absorption as well as strong cluster ionization [7, 8, 9, 10, 11]. However, when considering NIR laser pulses, the energy of the plasmon resonance in metallic as well as in preionized rare-gas clusters is typically well above the laser photon energy of 1.5 eV in early stages of the interaction. For example, a plasmon energy of about 4.0 eV is found for silver clusters [12] in the ground state and may be further increased by laser-induced inner ionization. Noting the density dependence of the Mie-plasmon energy ( $\omega_{\text{mie}} \sim \sqrt{\rho_{\text{I}}}$ , where  $\rho_{\text{I}}$  is the charge density of the ionic background), resonant collective heating requires a certain cluster expansion induced by ionization and non-resonant heating. Obviously, such sequence of ionization, expansion, and transient reso-

nance heating may be realized and resolved with very different pulse shapes, e.g., by excitation with a long pulse or with multiple well-separated pulses, respectively [13]. Likewise, the interaction process can be sensitively tuned by modifying the laser parameters, e.g., by changing the pulse duration, envelope, or chirp.

Indeed, several experiments have demonstrated that such simplified control techniques allow the enhancement of certain decay channels by optimizing the light field. In particular, cluster excitation with (i) stretched pulses having an optimal duration or with (ii) dual pulses having an optimal delay substantially support the generation of highly charged, energetic ions [14, 15, 16, 17] and fast electrons [18, 19]. At optimal pulse length, ion recoil energies can be further increased by (iii) introducing a weak additional shoulder in the leading edge of the laser pulse [20] or by (iv) using a negative pulse chirp [21].

As a next logical step, optimal control techniques based on iterative feedback with genetic algorithms can be used to further explore and optimize the cluster excitation process. Considering the strong pulse-structure dependence obtained in previous studies (i-iv), laser-cluster interactions provide ideal grounds to test and apply control schemes for steering the evolution of highly-excited many-particle system by a strong laser field. The first optimal control experiment on clusters in strong fields has been conducted by Zamith et al. [22], who used a liquid-crystal-based pulse shaper to maximize the abundance of highly charged Xe ions. The optimized light field contains a two-pulse sequence and produces ions up to  $\text{Xe}^{23+}$ . The spectral phase of the optimized laser field, however, was not analyzed.

In the present contribution we report on an optimal control experiment including a complete optimization and characterization of amplitude and phase of the laser field. As a prototype system we study silver clusters embedded in helium nanodroplets, which have shown a high

---

\*Electronic address: josef.tiggesbaeumker@uni-rostock.de

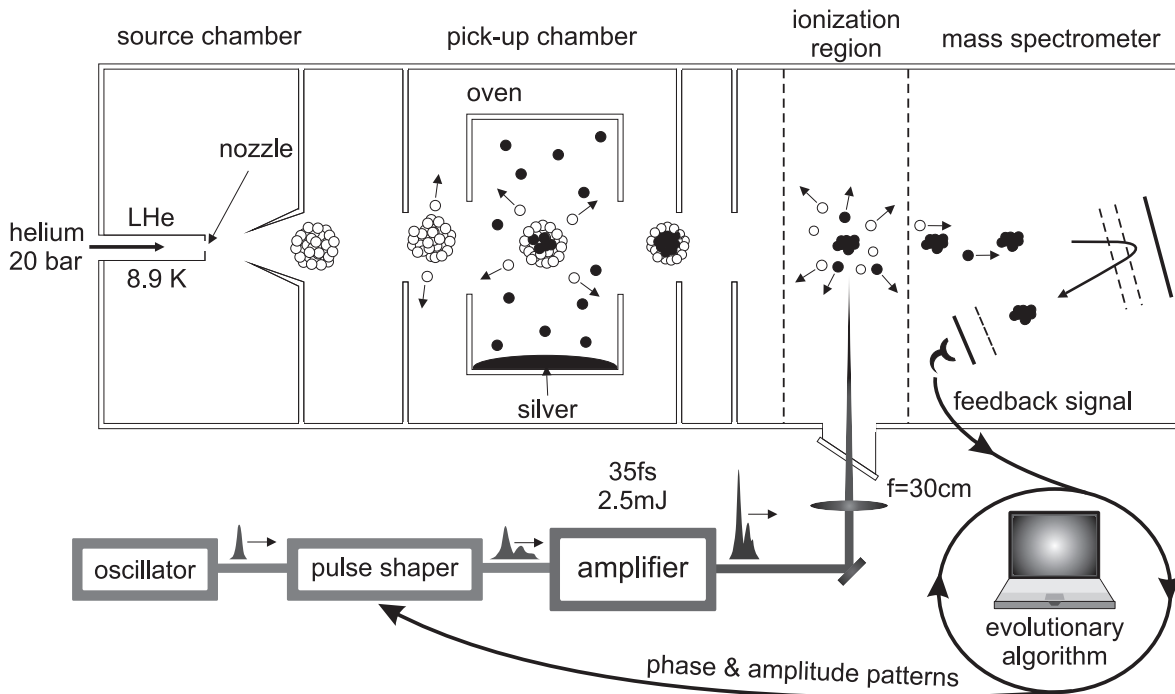


FIG. 1: Schematic view of the experiment: The top part visualizes the generation of the helium nanodroplets, the formation of the silver clusters inside the droplets by sequential atomic pickup in the oven, the laser excitation in the interaction region, and the time-of-flight analysis in the reflectron time-of-flight mass spectrometer (from left to right). The bottom part sketches the stages of pulse delivery from seed pulse generation in the oscillator, over pulse modification in the pulse shaper and final amplification, to pulse focusing into the molecular beam apparatus. In the optimal control experiment the yield of highly charged ions is maximized by applying an evolutionary algorithm scheme within a feedback loop (see arrows).

pulse-structure sensitivity in previous experiments [15]. For this metallic system collective electron motion is expected to dominate the optical absorption. In order to maximize the abundance of highly charged  $\text{Ag}^{q+}$  ions a multi-parameter genetic algorithm procedure is used for tailoring the pulses. A sketch of the experimental procedure is displayed in Fig. 1.

To evaluate the effect of the optimization, the resulting ion yields are compared to the spectra produced with bandwidth-limited and dispersively stretched pulses. The optimal pulse shapes are characterized by frequency-resolved optical gating (FROG) [23] and compared to results from a computational control experiment. The numerical optimization, based on a modified nanoplasma model [24], varies the pulse envelope function and is performed for a simplified system, i.e., pure silver clusters.

The remainder of the text is organized as follows. Section II describes the experimental methods, i.e., the cluster generation, the laser system, and the details of pulse shaping and characterization. The results of the experimental and numerical closed-loop optimizations are presented in Sec. III. The discussion and comparison of the data are subject of Sec. IV. Finally, conclusions are summarized in Sec. V.

## II. METHODS

### A. Experimental setup

Silver clusters are produced by the helium droplet pickup technique [25], see Fig. 1. Superfluid helium nanodroplets are generated by means of a supersonic expansion of highly purified helium gas (He 6.0) at a stagnation pressure of 20 bars and a temperature of 8.9 K through a  $5\text{-}\mu\text{m}$  nozzle yielding a mean droplet size of  $10^6$  atoms. After differential pumping the molecular beam enters the pickup region where silver atoms are loaded into the droplet, forming clusters consisting of up to 150 atoms [26]. By changing the nozzle temperature and the metal vapor pressure in the pickup cell, the size of the droplet as well as the size of the metal core can be varied nearly independently over a broad range. We note that this type of cluster source shows an outstanding long-term stability, which is a central requirement for performing the optimization experiments.

A Ti:Sapphire laser system, consisting of the oscillator, the pulse shaper, and the pulse amplifier, see Fig. 1, delivers pulses with energies of up to 2.5 mJ and pulse durations down to 35 fs (*full width half maximum*. FWHM) at 1 kHz repetition rate. Laser pulses enter the interaction region perpendicularly to the cluster beam and are

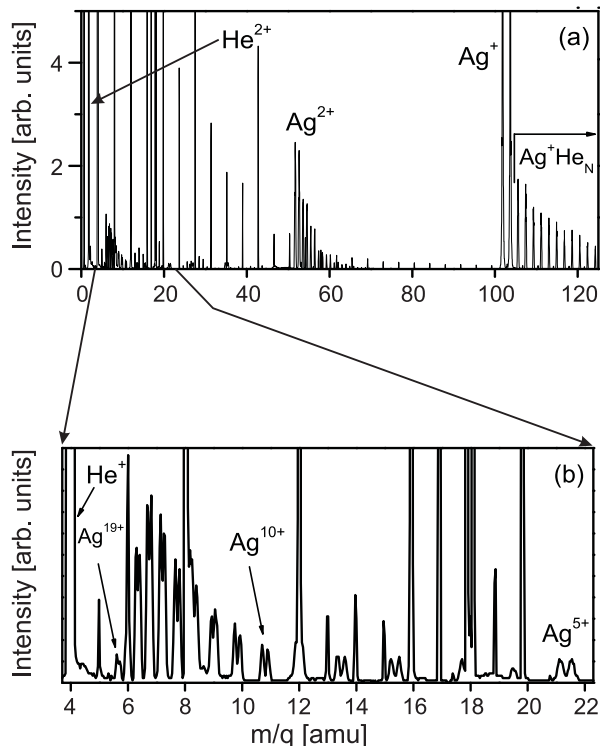


FIG. 2: Time-of-flight mass spectrum resulting from excitation of silver clusters in helium droplets by stretched 500 fs laser pulses at intensity  $7 \times 10^{14} \text{ W/cm}^2$  (top panel: overview; bottom panel: enlarged section highlighting the range from  $\text{Ag}^{5+}$  to  $\text{Ag}^{19+}$ ). The double peak structure of individual ion peaks results from the isotopic pattern of the silver atom ( $^{107}\text{Ag}$ ,  $^{109}\text{Ag}$ ). Due to the high recoil energies from the cluster Coulomb explosion the Ag ion features are broadened but can still be clearly resolved with the chosen detection technique. In addition to  $\text{Ag}^{q+}$ , also  $\text{He}^+$ ,  $\text{He}^{++}$ , helium cluster ions, and  $\text{Ag}^{q+}\text{He}_N$  are observed.

focused by a 30 cm lens ( $f^\# = 30$ ) to intensities of up to  $10^{16} \text{ W/cm}^2$ . Ions resulting from the laser-cluster interaction are accelerated by a static electric field of 2 kV/cm and analyzed by reflectron time-of-flight mass spectrometry [27]. Fig. 2 shows a typical mass spectrum resulting from excitation of the embedded metal complexes with 500 fs pulses at intensity  $I_0 = 7 \times 10^{14} \text{ W/cm}^2$ . The progression of multiply charged  $\text{Ag}^{q+}$  ions with  $q$  up to 19 can clearly be resolved with the applied detection technique, see Fig. 2(b).

### B. The Pulse Shaper

The oscillator delivers seed pulses with a spectral bandwidth of 50 nm (FWHM). Before amplification the pulses enter an acousto-optic programmable dispersive filter (AOPDF) (Dazzler, Fastlite) for pulse shaping, see Fig. 1. The shaper modulates both the amplitude and the phase

of the laser pulses simultaneously according to

$$E_{out}(\omega) \propto S(\omega)E_{in}(\omega), \quad (1)$$

with  $E_{in}(\omega)$  and  $E_{out}(\omega)$  the input and output laser fields in the frequency domain, and  $S(\omega)$  the frequency response function of the filter. Arbitrary femtosecond laser pulse shapes can be generated with the appropriate  $S(\omega)$  by controlling the acousto-optical signal. The frequency response function reads

$$S(\omega) = A(\omega) \exp[iB(\omega)], \quad (2)$$

where  $A(\omega)$  and  $B(\omega)$  are real functions describing the spectral amplitude and phase modulation, respectively. The AOPDF allows to realize a maximum group delay of 3 ps with 0.6 nm spectral resolution. For a more detailed description see Refs. [28, 29]. In our setup,  $A(\omega)$  and  $B(\omega)$  are defined by 60 parameters (30 in the range  $[0, 1]$  for  $A(\omega)$  and 30 in the range  $[0, 2\pi]$  for  $B(\omega)$ ) equally spaced over the spectral range.

In the control experiments these parameters are varied to optimize the pulse structure. We use an extended evolutionary algorithm scheme [30] to find the optimal laser pulse that maximizes the yield of highly charged atomic ions. For each pulse shape the mass spectrum is averaged over 6000 laser shots, whereas 50 individual laser pulse shapes enter each optimization cycle. The population of different pulse shapes is divided into separate sub-populations whose constituents are subject to crossover and random mutation after each generation. This procedure has been proven to be more robust and efficient when compared to simple genetic schemes [31]. The evolutionary process is iterated until the fitness value levels out. A full optimization experiment roughly takes 3-4 hours. The final result of the optimization procedure, i.e., the laser pulse structure yielding the highest fitness value, is fully characterized in amplitude and phase by a home-build frequency-optical-gating (FROG) analyzer [23].

## III. RESULTS

### A. Experimental findings

A comparison of the ion spectra resulting from excitation of the embedded silver clusters with (i) bandwidth-limited, (ii) optimally stretched, and (iii) fully shaped laser pulses is given in Fig. 3. The data in Fig. 3(a) shows a spectrum for cluster excitations with 50 fs pulses (i) at peak intensity  $I_0 = 10^{16} \text{ W/cm}$ . In this case the ion signal is dominated by  $\text{He}_N$  ions and weakly charged species of residual gas molecules (e.g.,  $\text{C}^{2+}$ ). Zooming in, however, reveals the generation of highly charged silver ions up to  $\text{Ag}^{17+}$  from the clusters with low yields, e.g., with about  $1.5 \times 10^{-3}$  ions per laser shot for  $\text{Ag}^{17+}$ . From previous studies it is well-known that longer pulses enhance the ion yield, see e.g. [14]. We utilize the AOPDF to stretch the pulses (ii) by introducing a linear temporal

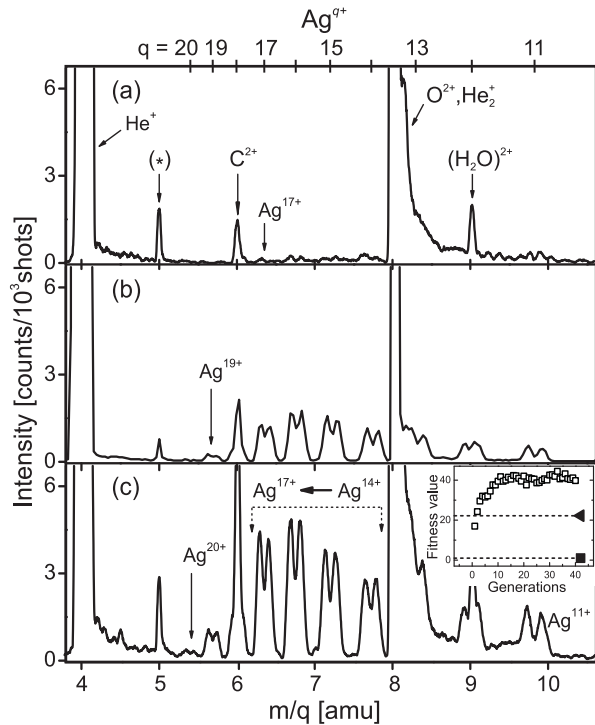


FIG. 3: Mass spectra with highly charged atomic ions obtained when exposing embedded silver clusters to intense laser pulses of different pulse shapes: (a) 50 fs pulses; (b) 500 fs linearly down-chirped pulses (cf. Fig. 2); (c) laser pulses fully optimized in amplitude and phase within the control experiment. Note, that the scales are directly comparable. Obviously the yield of  $\text{Ag}^{q+}$  is substantially enhanced with the tailored pulses. The inset in (c) shows the evolution of the average fitness value in the optimization experiment, i.e., the total yield of  $\text{Ag}^{q+}$  ( $q=14-17$ ) (open squares) compared to the reference measurements (50 fs: full square; 500 fs pulses: full triangle).

down-chirp on the frequency component. This results in a substantial increase in the yield of multiply-charged species from the clusters while ion contributions from background gas decline. At a pulse width of about 500 fs ( $I_o = 10^{15} \text{ W/cm}^{-2}$ ), see Fig. 3(b), we observe the maximal signal of  $\text{Ag}^{q+}$ , indicating optimal ionization conditions with a single pulse.  $\text{Ag}^{19+}$  shows up in the spectrum as the highest charge state. The two single-pulse measurements (i, ii) serve as references for the optimization experiments.

For the full optimization procedure (iii) the yield of  $\text{Ag}^{q+}$  ( $q = 14-17$ ) is taken as fitness value for the genetic algorithm. The resulting final mass spectrum is given in Fig. 3(c). The evolution of the fitness value (see inset) shows that the pulse structure quickly adapts to the details of the cluster dynamics. The fitness value exceeds the value for the optimally stretched single pulse (solid triangle) already after a few iterations. Subsequently, the fitness value begins to level out and saturates at about twice the stretched pulse value. Hence, the high- $q$  ion yield with the fully shaped light field is enhanced by

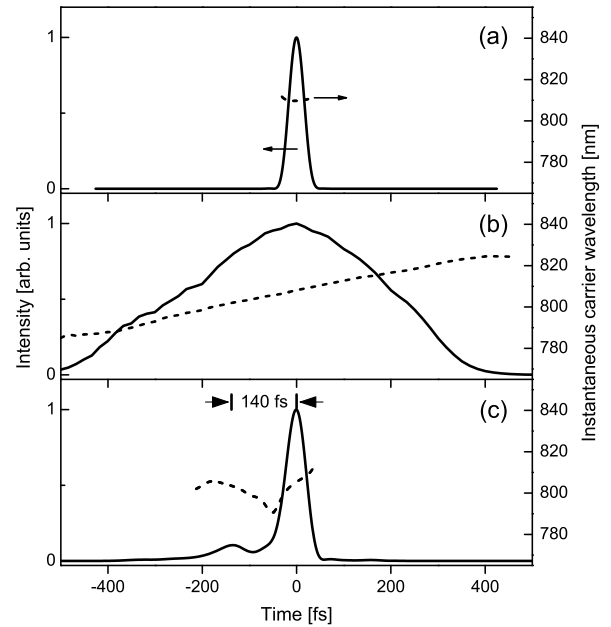


FIG. 4: Pulse shape (solid) and evolution of the carrier wavelength (dashed) of the laser fields corresponding to the three excitation scenarios in Fig. 3: (a) 50 fs pulse; (b) 500 fs linearly down-chirped pulse; (c) fully optimized light field. The tailored laser field leading to the enhanced generation of highly charged ions exhibits a double pulse structure, comprised of a weak, slowly rising prepulse and a stronger main pulse separated by 140 fs.

more than a factor of two when compared to the optimal single pulse, see Fig. 3(b) and (c). The increase is even more pronounced (factor 17) when comparing to the spectra for the shortest and thus most intense pulse, cf. Fig. 3(a). In addition, we also observe an increase in the highest charge state reaching  $q_{max} = 20$  with the fully optimized pulse shape.

As a first step towards unraveling the underlying dynamics, the pulses from the three excitation scenarios in Fig. 3(a)-(c) have been characterized in amplitude and phase, see Fig. 4(a)-(c). For convenience, the temporal intensity is given (solid) together with the phase evolution in terms of the instantaneous carrier wavelength (dashed), which is derived from the instantaneous angular frequency  $\omega(t) = \omega_0 - \dot{\phi}(t)$ , with  $\omega_0$  being the central angular frequency and  $\phi(t)$  the temporal phase of the pulse [23].

Whereas the flat evolution of the instantaneous carrier wavelength in Fig. 4(a) underlines excitation with a nearly bandwidth-limited pulse, the linear wavelength shift in Fig. 4(b) reflects the dispersive pulse stretching. The analysis of the optimized laser field, see Fig. 4(c), shows a simple double-pulse intensity distribution (solid line). A prepulse containing about 15% of the pulse energy excites the clusters prior to the main pulse. The

pulse intensity drops significantly between the subpulses, indicating a two-step excitation process to induce the effective generation of high charge states. This signature of the pulse is found to be rather robust with respect to the chosen pulse energy, i.e., the pulse delay as well as the intensity ratio may change while the general shape is preserved. Note that the optimization procedure introduces a substantial red-shift of the instantaneous carrier wavelength from 790 nm to 810 nm during the main pulse, see dashed curve in Fig. 4(c).

## B. Computational results

To assist the experimental study, we apply a theoretical approach to find laser pulse shapes that maximize the yield of highly charged ions in the laser-cluster interaction. For this purpose, a genetic algorithm is used and adapted to the nanoplasma approach of Ditmire [7]. The model contains the essential physical processes like ionization, heating and expansion. Briefly, the clusters are assumed to have uniform temperature and density profiles and are initialized as neutral spheres. To model the nanoplasma inner ionization dynamics, tunneling as well as electron impact ionization are taken into account. Heating via inverse bremsstrahlung, being the dominant process for laser energy capture, is described with effective rates for collisional absorption. The cluster expansion and the resulting cooling of the system are calculated using hydrodynamic equations. In our version of the nanoplasma model, plasma heating is treated by a generalized quantum statistical expression for electron-ion collisions including resonant collective absorption [32]. In addition, damping due to electron collisions with the cluster boundary, i.e., surface friction, is incorporated by including a corresponding collision term [33, 34]. Furthermore, the lowering of the ionization energies due to screening is taken into account [24].

To calculate the optimal light field for producing a maximum yield of specific ion species a genetic feedback algorithm is applied. For the optimization procedure, a pulse intensity shape  $I(t)$  according to the Ansatz

$$I(t) = \sum_{n=0}^4 A_n \exp \left[ -\frac{4 \ln 2 (t - t_n)^2}{\sigma_n^2} \right] \quad (3)$$

is used, with  $A_n$ ,  $t_n$ , and  $\sigma_n$  being the weights, time offsets, and temporal width parameters (FWHM) of the individual terms. Note that a fixed carrier wavelength of 810 nm is used in the calculations, i.e., the phase evolution is not optimized. The total pulse fluence is kept constant for each chosen pulse-shape and corresponds to a 810 nm Gaussian pulse of 35 fs (FWHM) with peak intensity  $1 \times 10^{16}$  W/cm<sup>2</sup>. Further, a lower limit of 35 fs is used for the width parameters  $\sigma_n$ . To calculate the best pulse shape, 20 different pools, each with a population of 40 species, are used in the optimization procedure.

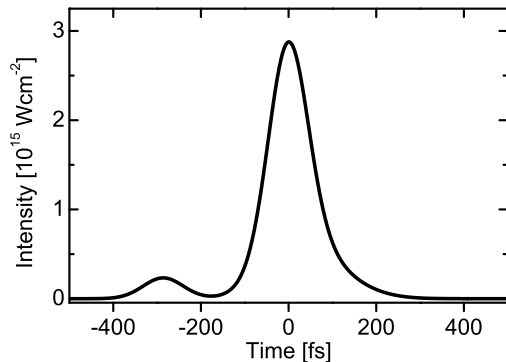


FIG. 5: Calculated temporal intensity evolution of the optimal light field for producing a maximum yield of  $\text{Ag}^{10+}$ . The intensity envelope is in qualitative accordance with the experimental result, cf. Fig. 4. The total pulse fluence corresponds to a 35 fs pulse with peak intensity  $1 \times 10^{16}$  W/cm<sup>2</sup>.

We perform the calculations as close as possible to the experimental conditions. Silver clusters with an initial radius of 2.5 nm (4500 atoms) are considered since smaller particles cannot be treated adequately within the nanoplasma model. The calculated optimal pulse shape giving the maximum yield of  $\text{Ag}^{10+}$  is shown in Fig. 5. This ion species was chosen because higher ionization levels were only weakly populated. Here, further improvements of the model would be necessary. For a discussion of additional processes to be included, like the enhancement of electron impact ionization by local cluster fields and the influence of the experimental setup, especially the frustration of recombination by the ion extraction electric fields after the laser pulse, see Ref. [35].

As references to assess the results of the genetic algorithm, calculations were also performed for a single 500 fs pulse and for a dual-pulse excitation scheme. Whereas the single pulse mainly produces  $\text{Ag}^{7+}$  and  $\text{Ag}^{8+}$ ,  $\text{Ag}^{8+}$  and  $\text{Ag}^{9+}$  are the dominant contributions in the ion spectra for dual pulse excitation. With the light field from the computational control experiment, see Fig. 5, the  $\text{Ag}^{10+}$  yield is enhanced by a factor of four over the result for dual-pulse excitation and by more than a factor of eight over the result for the 500 fs single pulse. The simulations predict an optimized light field having a low-intensity prepulse followed by a more intense main pulse, in good agreement with the experimental control study. Even the intensity ratio between the two subpulses is nearly reproduced by the calculation.

## IV. DISCUSSION

The applied pulse shaping technique combined with a genetic algorithm has been shown to allow the enhanced

production of highly charged ions from strong-field laser-cluster interactions. Compared to simpler excitation schemes with bandwidth-limited or stretched pulses, the ion yields could be substantially increased. The laser field tailored in amplitude and phase thus offers an alternative and more efficient ionization pathway.

We find that a sequence of a weak prepulse followed by a much stronger main pulse after about 140 fs leads to the highest ionization under the experimental boundary conditions. Interestingly, the bandwidth-limited pulse from the reference scenario and the main feature of the optimized light field are similar in intensity and duration. This underlines the decisive effect of the low-intensity prepulse ( $10^{15}\text{W}/\text{cm}^2$ ) for enhancing the ionization efficiency by up to an order of magnitude. The optimized light field also outperforms optimally stretched single pulses (500 fs) by a factor of two in the ion yield.

The envelope of the tailored light field and comparison with the results for a bandwidth-limited pulse suggest that efficient energy transfer and strong ionization take place within the stronger main pulse. These findings can be related to previous dual pulse studies on  $\text{Ag}_N$  in He droplets [15], where a specific optical delay was found to maximize the highly charged ion yield for excitation with a pair of identical pulses. The optimization presented here extends these experiments. The control study not only underlines the importance of a certain pulse delay that matches the cluster expansion required for most efficient resonant collective heating, but also highlights the impact of the pulse intensity ratio. The genetic optimization shows that a less intense prepulse is favorable for preionization of the particle in order to launch the cluster expansion. Near resonance, the pulse adapts to maximum heating and strongest charging. This general scenario is corroborated by the fact, that the observed characteristic pulse structure is quite robust with respect to changes of the pulse energy.

The observed pulse shape shows similarities with the result of an earlier control experiment by Zamith et al. [22] on  $\text{Xe}_N$  ( $\bar{N} \approx 1.6 \times 10^4$ ). The authors also found an asymmetric dual pulse with a time separation of 146 fs. Although the pulse envelope indicates a similar scenario, the actual target conditions are quite different. In silver clusters the delocalized valence electrons already form a metallic state, whereas a rare-gas system requires preionization for the nanoplasma formation.

Comparing the outcome of the present experimental optimization with the numerical one shows similar pulse structures. A detailed analysis of the simulation run for the numerically optimized light field corroborates that the main energy transfer into the system takes place upon the passage of the plasmon resonance in the trailing main pulse. Here, the major fraction of the energy capture occurs leading to strong heating and finally to the formation of a large number of highly charged ions. The computational results thus support that the optimal light field "tries" to utilize most efficient plasmon enhancement ionization [14].

Interestingly, the analysis of the instantaneous phase

reveals a red-shift of the central carrier wavelength (down-chirp) during the main laser pulse, cf. Fig. 4(c). This behavior can be explained with dynamic frequency locking of the laser field to the plasmon. As the cluster expands, a down-chirped laser field allows extended frequency matching with the collective mode. For this to occur, however, the increase in the ion density due to cluster inner ionization has to be overcompensated by a sufficiently rapid cluster expansion.

Finally, we like to discuss the impact of the helium nanomatrix. Whereas helium is almost transparent at infrared wavelengths for low intensities, substantial ionization and heating may occur under the strong laser field. In our calculations the helium is not taken into account up to now due to the restricted dimensional approach of the nanoplasma model. Very likely, the surrounding helium droplet influences both the timing as well as the final ionization state of the cluster ions. Further improvements of the model for resolving the radial structure of the system are underway. As has been reported recently by Mikaberidze et al. [11] for embedded xenon clusters ( $\text{Xe}_{100}\text{He}_{1000}$ ), the presence of the helium nanomatrix results in a large contribution to the total energy absorption in a strong laser field. The impact of the helium matrix on the final charge state distribution of the cluster constituents as probed in our experiment, however, remains a challenging problem for future investigations.

## V. CONCLUSION

Amplitude- and phase-modulated pulses have been used to maximize the highly charged ion yield from silver clusters embedded in helium nanodroplets. A substantial increase is found when comparing to bandwidth-limited and optimally stretched pulses. The laser field resulting from the control experiment shows a two-pulse structure which is in fair agreement with the result of a computational optimization experiment based on the nanoplasma model. The shape and phase evolution of the optimized laser field indicate that the tailoring adapts to take advantage of the plasmon enhanced response. This proof of principle experiment on the metallic prototype system thus reveals a unique signature from collective electron excitations and their importance for controlling strong-field laser-matter interactions.

## Acknowledgments

Main parts of the helium droplet machine have been provided by J.P. Toennies and his group at the MPI Göttingen. Financial support by the Deutsche Forschungsgemeinschaft within the Sonderforschungsbereich SFB 652 is gratefully acknowledged.

- 
- [1] E. M. Snyder, S. A. Buzza, and A. W. Castleman Jr., *Phys. Rev. Lett.* **77**, 3347 (1996).
- [2] E. Springate, S. A. Aseyev, S. Zamith, and M. J. J. Vrakking, *Phys. Rev. A* **68**, 053201 (2003).
- [3] A. McPherson, B.D. Thompson, A.B. Borisov, K. Boyer, and C.K. Rhodes, *Nature* **370**, 631 (1994).
- [4] T. Ditmire, J. Zweiback, V.P. Yanovsky, T.E. Cowan, G. Hays, and K.B. Wharton, *Nature* **398**, 489 (1999).
- [5] U. Saalman, C. Siedschlag, and J. M. Rost, *J. Phys. B* **39**, R39 (2006).
- [6] T. Ditmire, R. A. Smith, J. W. G. Tisch, and M. H. R. Hutchinson, *Phys. Rev. Lett.* **78**, 3121 (1997).
- [7] T. Ditmire, T. Donnelly, A. M. Rubenchik, R. W. Falcone, and M. D. Perry, *Phys. Rev. A* **53**, 3379 (1996).
- [8] H.M. Milchberg, S.J. McNaught, and E. Parra, *Phys. Rev. E* **64**, 056402 (2001).
- [9] M. Kundu and D. Bauer, *Phys. Plas.* **15**, 033303 (2008).
- [10] U. Saalman and J.-M. Rost, *Phys. Rev. Lett.* **91**, 223401 (2003).
- [11] A. Mikaberidze, U. Saalman, and J. M. Rost, *Phys. Rev. A* **77**, 041201(R) (2008).
- [12] J. Tiggesbäumker, L. Köller, K.-H. Meiwes-Broer, and A. Liebsch, *Phys. Rev. A* **48**, R1749 (1993).
- [13] J. Zweiback, T. Ditmire, and M. D. Perry, *Phys. Rev. A* **59**, R3166 (1999).
- [14] L. Köller, M. Schumacher, J. Köhn, S. Teuber, J. Tiggesbäumker, and K.-H. Meiwes-Broer. *Phys. Rev. Lett.* **82**, 3783 (1999).
- [15] T. Döppner, Th. Fennel, Th. Diederich, J. Tiggesbäumker, and K.-H. Meiwes-Broer, *Phys. Rev. Lett.* **94**, 013401 (2005).
- [16] V. Kumarappan, M. Krishnamurthy, and D. Mathur, *Phys. Rev. A* **66**, 033203 (2002).
- [17] A. Heidenreich, I. Last, and J. Jortner, *Las. Phys.* **17**, 608 (2007).
- [18] Th. Fennel, T. Döppner, J. Passig, Ch. Schaal, J. Tiggesbäumker, and K.-H. Meiwes-Broer, *Phys. Rev. Lett.* **98**, 143401 (2007).
- [19] V. Kumarappan, M. Krishnamurthy, and D. Mathur, *Phys. Rev. A* **67**, 043204 (2003).
- [20] K. Mendham, J. Tisch, M. Mason, N. Hay, and J. Marangos, *Opt. Express* **11**, 1357 (2003).
- [21] Yuji Fukuda, Koichi Yamakawa, Yutaka Akahane, Makoto Aoyama, Norihiro Inoue, Hideki Ueda, and Yasuaki Kishimoto. *Phys. Rev. A* **67**, 061201(R) (2003).
- [22] S. Zamith, T. Martchenko, Y. Ni, S.A. Aseyev, H.G. Muller, and M.J.J. Vrakking, *Phys. Rev. A* **70**, 011201(R) (2004).
- [23] R. Trebino, *Frequency-Resolved Optical Gating: The Measurement of Ultrashort Laser Pulses*. Kluwer Academic, London (2000).
- [24] P. Hilse, M. Moll, M. Schlanges, and Th. Bornath, *Las. Phys.* **19**, 428 (2009).
- [25] A. Bartelt, J.D. Close, F. Federmann, N. Quaaas, and J.-P. Toennies, *Phys. Rev. Lett.* **77**, 3525 (1996).
- [26] Th. Diederich, J. Tiggesbäumker, and K.-H. Meiwes-Broer, *J. Chem. Phys.* **116**, 3263 (2002).
- [27] T. Döppner, Th. Diederich, A. Przystawik, N.X. Truong, Th. Fennel, J. Tiggesbäumker, and K.-H. Meiwes-Broer. *Phys. Chem. Chem. Phys.* **9**, 4639 (2007).
- [28] F. Verluise, V. Laude, Z. Cheng, Ch. Spielmann, and P. Tournois. *Opt. Lett.* **25**, 575 (2000).
- [29] DAZZLER, <http://www.fastlite.com>.
- [30] H. Pohlheim, *Evolutionäre Algorithmen: Verfahren, Operatoren und Hinweise für die Praxis*. Springer, Berlin (2000).
- [31] David E. Goldberg, *Genetic algorithms in search, optimization, and machine learning*. Addison-Wesley Professional, New York (1989).
- [32] Th. Bornath, P. Hilse, and M. Schlanges, *Contrib. Plasma Phys.* **17**, 591 (2007).
- [33] F. Megi, M. Belkacem, M. A. Bouchene, E. Suraud, and G. Zwicknagel, *J. Phys. B* **36**, 273 (2003).
- [34] S. Micheau, H. Jouin, and B. Pons, *Phys. Rev. A* **77**, 053201 (2008).
- [35] Th. Fennel, L. Ramunno, and Th. Brabec, *Phys. Rev. Lett.* **99**, 233401 (2007).